Applied Thermal Engineering 130 (2018) 865–876

Contents lists available at ScienceDirect

Applied Thermal Engineering

journal homepage: www.elsevier.com/locate/apthermeng

Research Paper

Evaluation of heat transfer at the cavity-polymer interface in microinjection moulding based on experimental and simulation study

Maksims Babenko [a,*], John Sweeney [a], Petko Petkov [b], Franck Lacan [b], Samuel Bigot [b], Ben Whiteside [a]

[a] Centre for Polymer Micro & Nano Technology, Faculty of Engineering and Informatics, School of Engineering, University of Bradford, Bradford, UK
[b] High-Value Manufacturing Research Group, Cardiff School of Engineering, Cardiff University, Cardiff, UK

HIGHLIGHTS

- High speed IR camera used to measure melt cooling during the micromoulding cycle.
- Effects of surface topography on cooling through laser machined sapphire windows analysed.
- Experimental and simulation data compared to determine HTC value.
- Higher value of HTC improves cooling prediction for microinjection moulding.

ARTICLE INFO

Article history:
Received 27 February 2017
Revised 10 August 2017
Accepted 5 November 2017
Available online 8 November 2017

Keywords:
Heat transfer coefficient
Microinjection moulding
Polymer cooling
Simulation
Moldflow

ABSTRACT

In polymer melt processing, the heat transfer coefficient (HTC) determines the heat flux across the interface of the polymer melt and the mould wall. The HTC is a dominant parameter in cooling simulations especially for microinjection moulding, where the high surface to volume ratio of the part results in very rapid cooling. Moreover, the cooling rate can have a significant influence on internal structure, morphology and resulting physical properties. HTC values are therefore important and yet are not well quantified. To measure HTC in micromoulding, we have developed an experimental setup consisting of a special mould, and an ultra-high speed thermal camera in combination with a range of windows. The windows were laser machined on their inside surfaces to produce a range of surface topographies. Cooling curves were obtained for two materials at different processing conditions, the processing variables explored being melt and mould temperature, injection speed, packing pressure and surface topography. The finite element package Moldflow was used to simulate the experiments and to find the HTC values that best fitted the cooling curves, so that HTC is known as a function of the process variables explored. These results are presented and statistically analysed. An increase in HTC from the standard value of 2500 W/m^2 C to values in the region 7700 W/m^2 C was required to accurately model the observations.
© 2017 The Authors. Published by Elsevier Ltd. This is an open access article under the CC BY license (http://creativecommons.org/licenses/by/4.0/).

1. Introduction

Microinjection moulding is a leading technology for manufacturing polymer micro components in large quantities at a relatively low cost. Typically, masses of the final products can be less than 100 mg having dimensions in a micrometre range [1]. During the microinjection moulding cycle the polymer undergoes a complex process where it is heated to its melt temperature, injected at high velocity and high pressure into a cavity, where it cools down and solidifies into a final product. The heat transfer between the tool surface and the polymer melt has a significant influence on the filling and cooling behaviour. The flow of heat across this interface can influence the component form, surface properties, internal morphology, residual stresses and the dependent physical properties. This heat transfer is governed by the thermal contact resistance (TCR) or thermal contact conductance (TCC), (which is the inverse of the TCR) and is affected by the area of the contacting surfaces, the temperature of the polymer and mould, the pressure applied and the surface topography. Commercially available simulation software products use the term heat transfer coefficient (HTC) which is the same as the TCC.

The TCC is defined as the ratio of the heat flux (Q/A) to the additional temperature drop (ΔT) due to the presence of the imperfect joint and is defined as [2]:

$$TCC = Q/A\Delta T \ (W/m^2 \cdot K) \quad (1)$$

* Corresponding author.
E-mail address: m.babenko1@bradford.ac.uk (M. Babenko).

https://doi.org/10.1016/j.applthermaleng.2017.11.022
1359-4311/© 2017 The Authors. Published by Elsevier Ltd.
This is an open access article under the CC BY license (http://creativecommons.org/licenses/by/4.0/).

Heat flow through the interface of the contacting surfaces can be split into the three forms, namely conduction through the contact spots, conduction through the microscopic or macroscopic voids between the actual contact spots (which can be filled with different conducting substances such as air, other gases, coatings and greases) and radiation across the gaps (which can be ignored if the temperature at the interface is lower than 400 °C). Convection can be disregarded because the interfacial gap thickness is so small [2–4].

The heat transfer at polymer/metal interfaces has been studied previously by a number of researchers. Steady state experiments were performed by Marotta and Fletcher [5], Narh and Sridhar [6] and Dawson et al. [7] using an axial heat flow apparatus, described elsewhere [8]. Results were reported for a range of polymers and range of substrates. The HTC values were varying between 250 and 1659 W/m^2 K in the work of Marotta and Fletcher [5], 15,000 and 25,000 W/m^2 K in the work of Narh and Sridhar [6] and around 7000 W/m^2 K in the work of Dawson et al. [7]. The suggested values of HTC at metal-polymer interfaces in [5–7] were obtained on solid polymer samples through steady state experiments, with relatively low applied pressures when compared with those typically seen in microinjection moulding.

In conventional injection moulding Yu et al. [9] determined HTC values for Acrylonitrile butadiene styrene (ABS)/steel interfaces with sample thicknesses in the range of 2–4 mm and showed the HTC dependence on material properties, processing conditions and the thickness of the part. Sridhar and Narh [10] through their work showed that HTC is transient, which was confirmed in later study by Sridhar et al. [4]. Delaunay and Le Bot [11] have proven experimentally that constant mould temperature cannot be used as a boundary condition for injection moulding simulation and perfect contact between the polymer and the mould cannot be assumed either. When the cavity pressure reaches zero a sudden decrease in HTC occurs, which can be explained by considering the gap formation between the cavity wall and the polymer surface due to shrinkage of the polymer part. Observation in the work of Sridhar et al. [4] and Delaunay and Le Bot [11] were confirmed by Bendada et al. [12–13], who have designed a novel system for measuring polymer temperature during the injection moulding cycle and have shown in their work that HTC does not change when high pressure is applied, but when pressure drops to zero, HTC suddenly decreases. Masse et al. [14] studied the cooling stage of polymer within an injection moulding process, taking into account parameters such as HTC, residual stresses, and the PvT diagram. They have tested three surfaces with different roughness (Ra = 0.05 μm, Ra = 1 μm, Ra = 5 μm) at different pressures. Results showed that HTC decreases when roughness increases.

Up to this point all the experimental work was conducted using conventional injection moulding machines and on relatively large parts with wall thicknesses greater than 1 mm. A limited amount of research has considered HTC in microinjection moulding. Nguyen-Chung et al. [15] focused on determination of HTC during the filling stage in microinjection moulding through a short-shot study on parts with wall thicknesses of 0.2 mm and 0.5 mm. The experimental work showed that cavity pressure, thickness of the cavity and injection speed has an effect on HTC. Values of the heat transfer coefficient for thicker components were lower compared with the thinner micro-spirals. For the thicker micro-spirals HTC was varying between 0 and 8000 W/m^2 K, whereas for the thinner sections it was in the range of 1500–25000 W/m^2 K. Somé et al. [16] focused their work on developing a model for prediction of HTC values in a steady state with varying pressure or in transient condition but with constant applied pressure. HTC values for polypropylene (PP) and ABS in contact with steel, chromium and polytetrafluoroethylene (PTFE) were experimentally obtained and modelled. The effect of surface roughness (Ra = 0.05 μm, Ra = 1 μm and Ra = 5 μm) was also investigated. It was shown that thermal conductance is higher for smooth surfaces and lower for rough surfaces. ABS/Steel HTC values for several surface roughnesses were varying from approximately 600–1600 W/m^2 K, PP/steel interfaces 600 – 10,000 W/m^2 K and ABS/steel, ABS/chromium and ABS/PTFE 900–1500 W/m^2 K. Liu and Gehde [17] focused their work on evaluation of HTC at the mould/polymer interface to improve the cooling and crystallinity simulation. The HTC values were determined for LDPE taking into account three different melt temperatures, three injection rates and three surface roughnesses, namely Ra = 0.01 μm, Ra = 1.36 μm and Ra = 5.81 μm. It was shown that the HTC increases with raising melt temperature and injection rate. It has to be noted that thickness of the part was 2 mm and was the same thickness that was used in Ref. [16], however the effects of the surface roughness reported were the opposite to those reported by Somé et al. Reported values of HTC were between 18,750 and 22,500 W/m^2 K for Ra = 0.01 μm, 26,000 – 33,000 W/m^2 K for Ra = 1.36 μm and 28,750 – 34,000 W/m^2 K for Ra = 5.81 μm. Hong et al. [18] determined HTC values at nickel/PMMA interface through a short-shot study measuring the filling height of the patterns on 1.12 mm thick samples with cylindrical micropatterns of 30 μm in diameter and 14 μm in height. The HTC values varied between 2300 and 10,000 W/m^2 K. At the present time, the availability of data to determine HTC in microinjection moulding is limited and despite its importance in solidification prediction it remains poorly understood.

A number of standard boundary condition values are used in injection moulding simulations, which may be unsuitable for microinjection moulding simulation and the heat transfer coefficient is one of them. The HTC values typically used in simulation were obtained from experiments performed with conventional injection moulding and typically with cavity thickness above 1 mm. Moreover, in the software, the HTC is assumed to have a constant value and then it cannot adequately describe the flow through micro channels [19].

In this study we have taken a novel approach in determination of HTC values for microinjection moulding. The work has included bespoke experimental mould design and manufacturing, materials characterisation, infra-red temperature measurements, and cooling analysis prediction using commercial simulation software.

We shall derive values of HTC as a function of mould surface topography, melt and mould temperature, injection speed and packing pressure. This will enable us to evaluate the effects that the customary assumption of a constant HTC value would have on the validity of micromoulding simulations. This has implications for injection moulding in general.

2. Experimental

In order to study polymer cooling directly, a special mould was designed based on a flow visualisation tool previously developed at the University of Bradford [20]. A transparent sapphire window was used as one half of the mould cavity. The fixed half of the mould was fitted with a 45° first surface mirror, which enabled visibility within the cavity through the sapphire window. The cavity pressure was measured using a Kistler 6189A p-T sensor (sensitivity = −6.450 pC/bar, linearity ≤ ± 0.15% full scale output) flush mounted in the centre of the cavity of the moving part of the mould.

2.1. Sapphire

The thermal properties of sapphire are very similar to P20 mould steel. Specifically, the thermal conductivity at 20 °C is 29 W/mK for P20 tool steel and 23 W/mK for sapphire. The specific

heat capacity at 20 °C is 460 J/kgK for P20 steel and 750 J/kgK for sapphire. The optical properties are well suited for the application, having a transmission range of 0.17–6.5 μm allowing measurements in the short to medium IR spectrum.

In order to study the effects of surface roughness on polymer cooling, sapphire windows were machined using an Oxford Lasers PicoLase 1000 micromachining system at Cardiff University [21].

A total of five sapphire windows were used in the experimental study. One of them was optically flat (N1), two roughened (N2, N3) and two structured with micro pillars (N4, N5). Their topography was analysed using Olympus LEXT OLS4000 laser confocal microscope. Z step standard sample (OLS4KC02), with Z = 1.94 μm, uncertainty (U) at a coverage factor k = 2 equal to 0.04 μm was used for calibration. Measured average error for MPLANON20X-LEXT objective lens was 0.057 μm. Z repeatability measurement was 0.002 μm. The evaluation area was selected based on the infrared camera's frame size of 128 × 128 pixels, which is equal to 1.92 × 1.92 millimetres. The average surface roughness was measured for sapphire windows N1, N2 and N3, whereas analysis of the sapphire windows N4 and N5 was based on the average height of 20 micro pillars randomly selected in the centre of the array. The surface roughness was calculated in terms of standard areal roughness parameters, namely the arithmetic mean of the absolute height within a sampling area (S_a) and the root mean square value of the ordinates within the sampling area (S_q), summarised in Table 1 [22].

2.2. Materials and equipment

A Battenfeld Microsystem 50 microinjection moulding machine was employed in this experimental study. The injection speed of the machine is controlled by servo-electric motor and verified with magnetostrictive linear position sensor (linearity < ± 0.01% full stroke minimum ±50 μm, repeatability < ± 0.001% full stroke minimum ±2.5 μm). The specimen investigated was a disk with diameter of 16.6 mm and thickness 0.5 mm shown in Fig. 1. Two commonly used materials in injection moulding, polypropylene (PP) 100-GA12 by Ineos and polystyrene (PS) 158 K by BASF, were selected to perform the planned design of experiments (DOE). Both materials are selective emitters and appear transparent to most IR wavelengths.

To overcome the IR transparency of the selected materials, they were compounded with 4 wt% carbon black (CB) masterbatch, as carbon materials show strong absorption in the IR region of the spectrum [23]. A Prism TSE 16 TC bench-top co-rotating twin-screw extruder was used for materials compounding. Fourier transform infrared spectroscopy (FTIR) and differential scanning calorimetry (DSC) were employed to analyse the effects of carbon black on the IR transparency and thermal properties of the compounded materials.

Infrared (IR) transmission and reflectance spectra for samples of both compounded materials were collected using a Nicolet iS50 FTIR spectrometer. The results for both materials showed that all IR light in Mid-IR range is absorbed, and the samples are highly IR opaque. The conclusion was made that addition of 4 wt% of carbon black masterbatch to PP and PS makes it possible to accurately measure the surface temperature of the polymer melt during the microinjection moulding cycle.

A Discovery DSC by TA Instruments was used to analyse the melt temperatures (T_m) for PP and CB PP, the glass transition temperatures (T_g) for PS and CB PS, and measurement of heat capacity for all four materials. Temperature accuracy for the Discovery DSC is ±0.025 °C, temperature precision ±0.005 °C, heat flow noise (rms) ≤0.08 μW, baseline linearity (−50 °C – 400 °C) ≤ 5 μW baseline accuracy ±20 μW, baseline repeatability ±5 μW. The addition of 4% carbon black masterbatch did not affect the T_m of polypropylene, as only a change of 0.02 °C was observed. Measured T_g for PS was 102.75 °C and 102.12 °C for CB PS respectively. Observations of T_g range and midpoint for PS and CB PS suggest that addition of carbon black masterbatch does not affect T_g significantly. The heat capacity of polymers was measured using modulated differential scanning calorimetry (MDSC). Results showed that the addition of pigment to polystyrene was statistically insignificant. In the case of polypropylene, the increase of heat capacity was observed with an addition of carbon black masterbatch. The highest increase of heat capacity (12.7%) was observed at a low temperature of 16.85 °C. With an increase of temperature, the difference in heat capacities between carbon black filled and neat polypropylene was 6.8% at 186.85 °C.

2.3. High speed IR camera

An ultra high speed, high sensitivity infrared camera FLIR X6540SC was used for the experimental work. The camera has a cooled Indium antimonide (InSb) focal plane array (FPA) detector with the spectral range of 1.5–5.1 μm, pixel pitch of 15 μm and aperture of F/3. The detector sensitivity (NETD) is <20 mK at 25 °C which can capture a temperature difference of less than 20 mK (0.02 °C). Calibration of materials and further experiments were performed with a frame size of 160 × 128 pixels (2.4 × 1.92 mm), integration time of 50 μs and frame rate of 1000 frames per second.

2.4. Materials calibration

The optical train of the visualisation system is quite complex due to multiple reflections, absorption and emissivities of each element. Therefore, it is impractical to compensate for the IR attenuation analytically. Instead, the system was calibrated empirically using the following method:

- The mould temperature was set to a predetermined value and allowed to stabilise.
- Polymer was injected into the cavity.
- The material remained in the cavity for 5 min to thermally stabilise (mould was closed
- The camera's digital level (DL) value was recorded.
- The mould was opened and the polymer part remove

Table 1
Sapphire windows topography.

	S_a (μm)	S_q (μm)	Evaluation area (μm)		Area (mm²)	Effective surface area (mm²)
N1 (Polished)	0.007	0.011	1920 × 1920		3.68	3.68
N2 (1 μm)	1.089	1.335	1920 × 1920		3.70	5.08
N3 (4.2 μm)	4.214	5.091	1920 × 1920		3.71	7.88
	Average height (μm)		Standard Deviation (μm)	Number of Pillars		
N4 (15 μm pillars)	15.14		0.277	20	3.70	5.20
N5 (30 μm pillars)	33.2		1.245	20	3.70	15.05

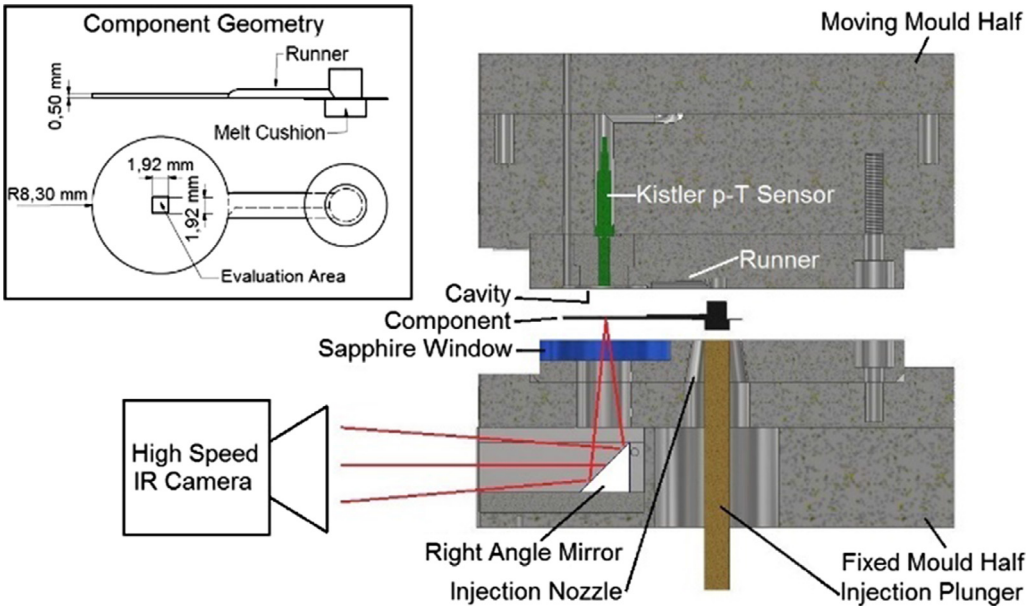

Fig. 1. Schematic of the visualisation system and component geometry.

This process was performed over a temperature range of 55 °C–200 °C, in 5 °C increments. The actual temperature of the polymer was verified with the p-T sensor mounted in the moving part of the mould. This data was used to create a calibration curve for the materials. Then a curve fitting algorithm, namely a fourth order polynomial, was fitted to the data points. The material calibration process is explained in more detail in Appendix A.

2.5. Design of experiments

A full factorial design of experiments was implemented, considering melt temperature, mould temperature, injection speed, packing pressure and surface roughness, as shown in Table 2. For each run, the first 20 parts were discarded. After 20 cycles the process was thermally stabilised and the subsequent 10 parts were collected together with recorded temperature and cavity pressure distributions. The cooling profiles and cavity pressure curves were averaged for each run.

2.6. Simulation

Three-dimensional filling, packing and cooling simulation was performed using Moldflow simulation software (2015, SP 2) [24]. Two cooling simulation methods provided by the software were investigated for the prediction of polymer cooling during the microinjection moulding cycle. These were the conduction solver, which employs a single value of HTC and a flow solver which employs a three-stage HTC for each of the filling, packing and cooling (detached) phases of the process. For the accuracy of the simulation a 3D mould together with part geometry was imported from CAD geometry and meshed to meet the demand of the simulation process. A different mesh size was used for part geometry and mould components according to the resolution required and the expected rate of temperature change in such areas. The part geometry was designed with a fine mesh (~1,900,000 elements), having a cavity volume of 232 mm^3 and identical volume of tetrahedral elements. The minimum number of elements through the thickness was selected to be ten. On the surface of the part that faces the sapphire window, a number of extra nodes was created. These were a set of 25 nodes within a 2 by 2 mm area in the middle of the part. The newly created nodes were then merged with the existing nodes from the part mesh. The temperature profile at each node was then exported and averaged to simulate experimentally obtained cooling profiles.

2.6.1. Governing equations

The governing equations employed in the software includes the conservation equation of mass, momentum, and energy [25]. Conservation of mass is represented by:

$$\frac{\delta \rho}{\delta t} + \nabla \cdot (\rho V) = 0 \tag{2}$$

where ρ is the polymer density, t is time and V is the velocity vector. For conservation of momentum:

$$\rho \frac{DV}{Dt} = -\nabla P + \nabla \cdot \tau + \rho g \tag{3}$$

Table 2
Factors and level settings for CB PP and CB PS DOE.

Factors and level settings (CB PP and CB PS)						
Factors	Name	Level 1	Level 2	Level 3	Level 4	Level 5
A	Surface Roughness	0.007 μm	1 μm	4.2 μm	15 μm pillars	30 μm pillars
B	Melt Temperature	220 °C	240 °C			
C	Mould Temperature	60 °C	80 °C			
D	Injection Speed	200 mm/s	500 mm/s			
E	Packing Pressure	300 bar (CB PP)/500 bar (CB PS)	600 bar (CB PP)/1000 bar (CB PS)			

where P is pressure, τ is the viscous stress tensor and g is the gravitational acceleration vector (insignificant in micromoulding studies). For conservation of energy:

$$\rho C_p \frac{DT}{Dt} = \nabla \cdot (k\nabla T) + \nabla V + \beta T \frac{DP}{Dt} \quad (4)$$

where k is the polymer thermal conductivity, C_p is the specific heat capacity of the melt and β is the polymer expansivity which is defined as:

$$\beta = -\frac{1}{\rho}\frac{\delta \rho}{\delta T} \quad (5)$$

At the polymer-mould interface, the equivalent of Eq. (4) includes HTC. There is a discontinuity in temperature ΔT at the interface and for energy flow normal to it,

$$Q/A = (HTC)\Delta T \quad (6)$$

where Q/A is the heat flow per unit area.

The equations are solved by using a finite element method and the Galerkin approximation. Flow inlet node is defined on the surface corresponding with that formed by the end of the injection piston. Boundary conditions are determined depending on the type of thermal solver used as defined in the next section of this paper.

2.7. Conduction solver

The conduction solver is the default solver for part heat flux calculations in Moldflow. Results of the temperature distribution are available through the "Cool" (FEM) analysis sequence. Because the conduction solver assumes that the cavity is instantly filled with polymer melt, there are only two boundary conditions that can be specified, namely melt and mould temperatures. The effects of injection speed and packing pressure are not taken into account, so the 16 runs of the experimental DOE could be simulated with just four runs here. The conduction solver uses the packing HTC value for the cooling phase. This is based on the assumption that the filling phase is of much shorter duration compared to the packing phase. Moreover, the Cool analysis cannot determine whether the part has detached or not. The whole part or a particular area can be selected and assigned local heat transfer coefficients through the "Part surface properties" option.

2.8. Flow solver

In the flow solver, filling and packing parameters can be specified in addition to the melt and mould temperatures which are determined dynamically throughout the cycle by calculating heat flux through the polymer, across the interface and through the mould components at each time step. Default values were used for considering flow across the interface between mould components and for losses to the environment through convection at external mould surfaces. During the analysis, pressure in the cavity is computed at each time step so that the detached condition is also known. The part temperature distribution results are available by setting Cool (FEM) + Fill + Pack analysis. However, the temperature results from the Fill + Pack solver refer to the mould temperature at the interface rather that the polymer temperature for surface nodes. The polymer temperature on the surface nodes is available by modification of the software "dat" files. This adds an extra function for the Fill + Pack solver, which writes an additional time series (XY) result for selected surface nodes representing the true polymer temperature. The flow solver employs three-stage HTC values, for filling, packing and the detached condition which is intended to provide more accurate results compared to the conduction solver. If the HTC values are not changed the software will use default values of 5000 W/m^2 C for filling, 2500 W/m^2 C for packing and 1250 W/m^2 C for the detached phase. These values can be changed through the "part surface properties" option, by assigning local HTC values.

3. Results and discussion

3.1. Experimental cooling profiles

In this study we were primarily interested in the cooling behaviour of microinjection moulded components and associated HTC values. A full factorial design of experiments focusing on the processing parameters and surface roughness was conducted aiming to enhance our understanding of the cooling behaviour and the HTC. Fig. 3 demonstrates two temperature distributions recorded with the IR camera. The only difference between the two cooling curves is the injection speed, where run 1 is 200 mm/s and run 3 is 500 mm/s. The temperatures measured are the peak temperature (filling) and average temperature (cooling) in the region of interest defined by the blue square in Fig. 3 (1.92 × 1.92 mm).

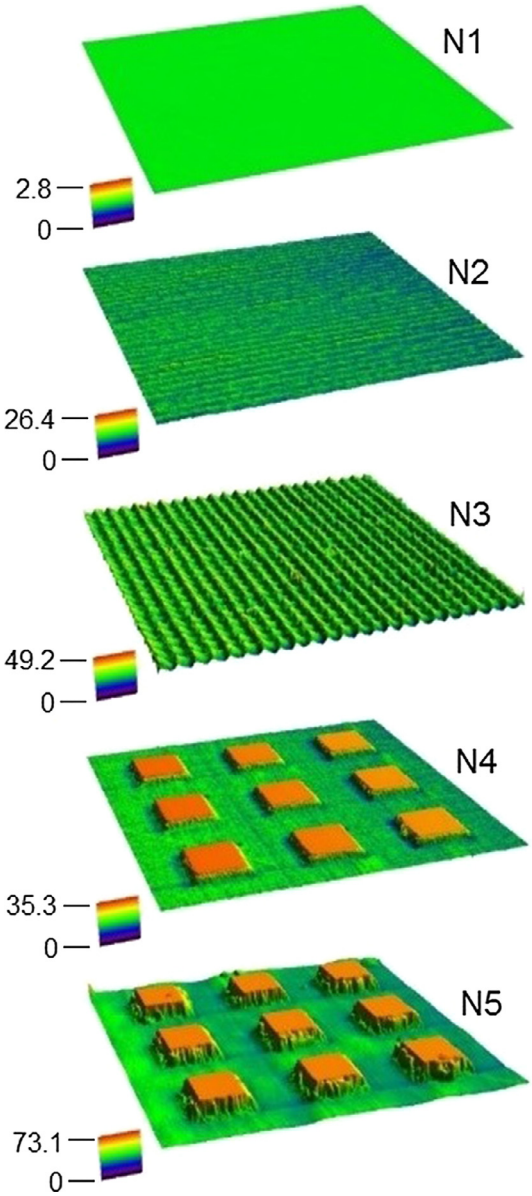

Fig. 2. Surface topography of five sapphire windows used as per Table 1.

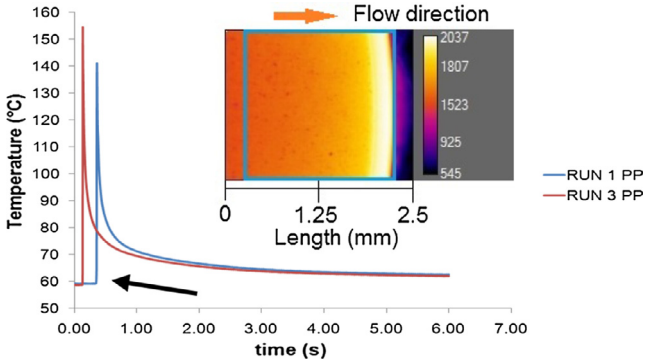

Fig. 3. Surface temperature curves recorded with the IR camera. t = 0 s at the start of injection.

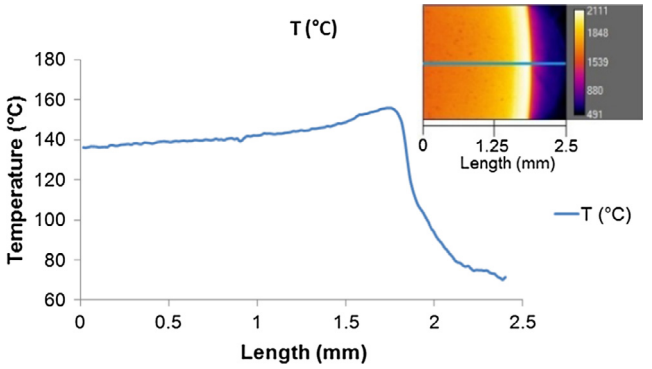

Fig. 4. Temperature distribution of a single line of pixels (inset) plotted as a distance from the left edge of the acquisition window.

The black arrow shows the temperature before the injection, i.e. the mould temperature. These two curves cannot be compared directly, because with higher injection speed polymer melt reaches the centre of the cavity faster, so that peak temperatures are misaligned. To compare cooling curves directly they were aligned to their peak temperatures, therefore t = 0 is at the peak temperature measured.

The peak average temperature measured is nowhere near the melt set temperature of 220 °C. The melt touches the cold surface and cools down extremely rapidly. This can also be observed during cavity filling shown in Fig. 4 which shows a line profile across the region of interest. The difference between the flow front and material approximately 2 mm behind is nearly 20 °C.

Another interesting observation is that flow front temperature decreases further as it moves into the cavity. Fig. 5 shows eight frames captured during the filling centre of the cavity. In the graph line profiles are plotted together with the maximum temperature values. The geometry of the part is 16.6 mm diameter disk and what is plotted is an area in the centre of the disk (H = 1.92, W = 2.4 mm). This suggests that the temperature of the flow front is higher when it just starts filling the cavity. This is because thermal contact between the melt and cavity surface is initially poor and improves as the polymer fills the cavity.

3.2. Effects of processing conditions

The Minitab 16 analysis software was used to perform a statistical analysis of the peak surface temperature data. Significant effects were analysed depending on the temperature of the polymer at different time steps which are t = 0 s (peak T), t = 0.25 s, t = 0.5 s, t = 1 s, and t = 1.5 s. The Pareto chart shows that the most influential process parameters on the peak temperature during filling were injection speed, melt temperature and mould temperature, shown in Fig. 6 (left). Injection speed was found to be the most significant factor during filling for both materials CB PS and CB PP.

Fig. 6 (right) represents Pareto analysis of polymer temperature (CB PS) during cooling or at t = 0.25 s. With a confidence limit of 95%, it shows that mould temperature and melt temperature are both statistically significant parameters with the mould temperature being the most influential.

The main effect plot for the four factors (Melt T, Mould T, injection speed and Packing pressure) and two-levels for each factor for a range of surfaces, polished sapphire, 1 μm sapphire, 4.2 μm sapphire, 15 μm pillars sapphire and 30 μm pillars sapphire were also analysed. At t = 0 the effects of melt temperature, mould temperature and injection speed are clearly visible. The analysis of the temperature at t = 0.25 s, t = 0.5 s, t = 1 s, and t = 1.5 s suggests that mould temperature is the most influential parameter on polymer cooling for all the surfaces. Melt temperature is less significant, whereas injection speed and packing pressure remain virtually the same when comparing low and high levels as shown in

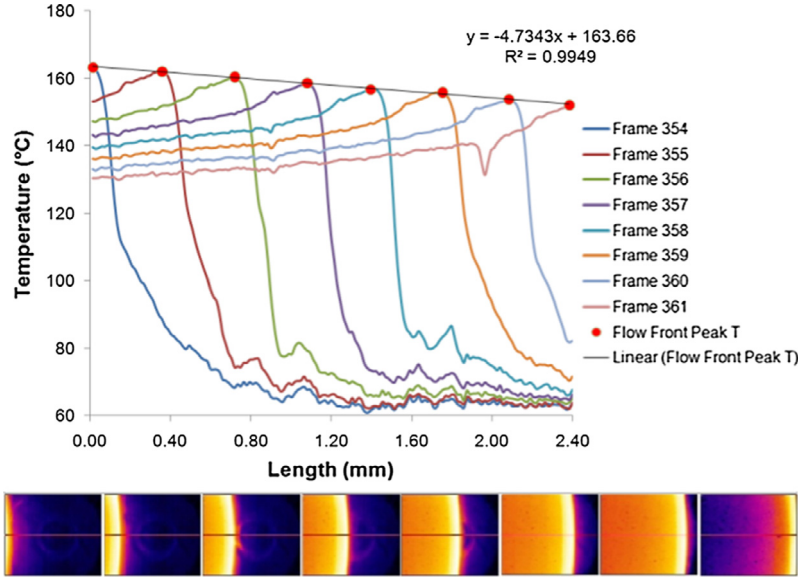

Fig. 5. Temperature distributions of pixel contours as defined in Fig. 4 for multiple frames recorded during cavity filling.

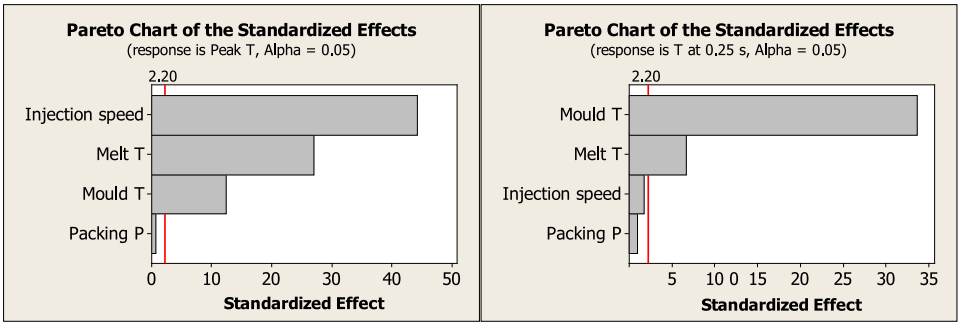

Fig. 6. Pareto analysis of the processing parameters during cavity filling CB PS (left) and polymer cooling CB PS (right).

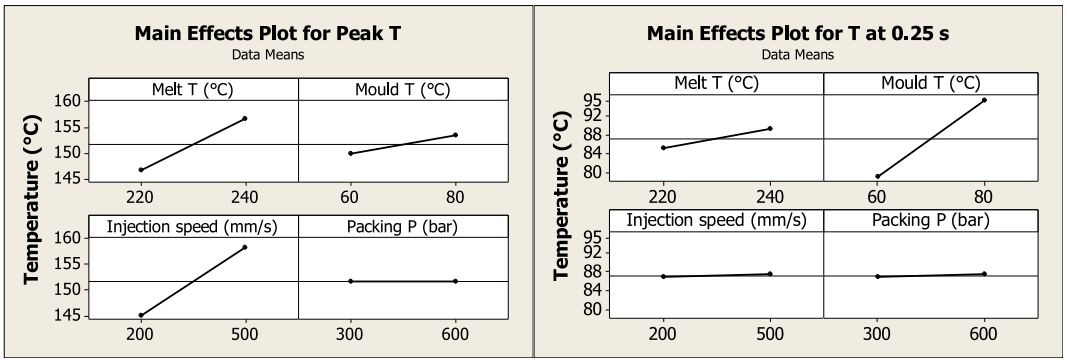

Fig. 7. The main effects plot of processing parameters on polymer temperature at t = 0 s (left), at t = 0.25 s (right).

Fig. 7. The effects of the processing parameters have followed the same trends for both materials and for the range of surface topographies.

3.3. Effects of surface topography

The effects of surface topography on polymer cooling were analysed separately. The effective surface area was measured using an Olympus LEXT OLS4000 laser confocal microscope. It was expected that high effective surface area would increase cooling rate. Fig. 2 shows the five surface topographies measured. An increase of effective surface area can be observed with an increase in surface roughness and height of the pillars, as expected (see Table 1). Fig. 8 represents average cooling rate curves for CB PS at low processing settings (T melt = 220 °C, T mould = 60 °C, Inj. Speed = 200 mm/s, Packing P = 500 bar). During cooling the maximum standard deviation was 1.68 °C for CB PS and 1.38 °C for CB PP. During the filling (Peak T) temperature deviation was higher; however, this was caused solely by the results from the 4.2 μm sapphire window. It was observed that for both materials peak temperatures recorded were lower for this window by 7–18 °C in comparison with all the others. This suggests that during filling of the cavity with a roughness of 4.2 μm, the melt loses heat more rapidly. Interestingly, the 1 μm sapphire and 15 μm pillars patterned into the sapphire have similar effective surface area, but the cooling results differ, which suggests that cooling is affected by surface topography, as well as effective surface area. A rise in the cooling rate curves around 0.02 s can be observed and it corresponds with an increase of pressure in the cavity as the cavity becomes completely filled. The rise was less pronounced for polished sapphire. The data suggests that the flat sapphire surface has good contact with the melt during the filling phase of the process and provides effective cooling in comparison to the other surfaces where the polymer may not have penetrated fully into the surface geometry to provide good thermal contact. However, when the pressure builds in the cavity at the switchover point between the filling and packing phases, it drives polymer flow into the micro asperities in the rougher surfaces, providing a larger effective area of contact and improved cooling in comparison to the flat sapphire reference.

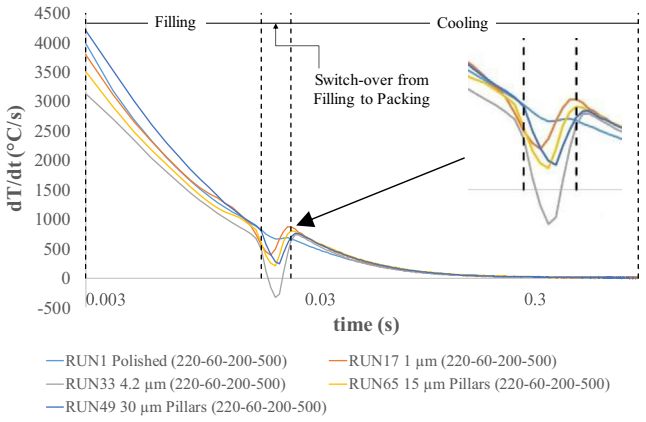

Fig. 8. Cooling rate curves for CB PS at low processing parameters (T melt = 220 °C, T mould = 60 °C, Inj. Speed = 200 mm/s, Packing P = 500 bar).

When comparing the cooling curves at high processing conditions (T melt = 240 °C, T mould = 80 °C, Inj. Speed = 500 mm/s, Packing P = 1000 bar) to cooling curves at low processing settings, no rise in cooling rate curves was observed. This suggests that due to the increased melt temperature, mould temperature and injection speed, viscosity of the melt is lower and there is no or minimal delay in polymer melt filling micro asperities. Fig. 9 shows the effects of surface topography on cooling behaviour for CB PS and CB PP. Each point represents an average temperature of 4 process-

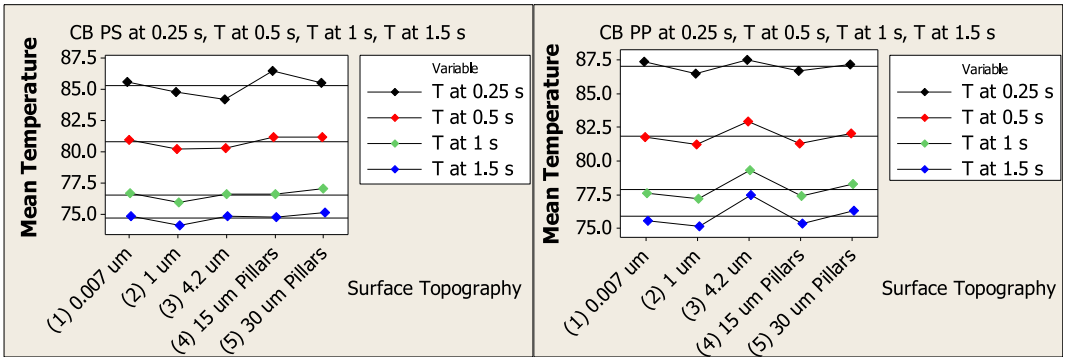

Fig. 9. The main effects plot of surface topography on polymer temperature for CB PS and CB PP.

ing conditions (T melt, T mould, Inj. Speed, Packing P) for each topography at variable time steps. Repeatable results can be observed for both materials when comparing the polished surface and 1 μm sapphire windows at all temperatures. The results for CB PP show consistently that surface temperature for 4.2 μm surface was higher comparing to the polished and the 1 μm rough surfaces. It was expected that due to higher effective surface area the mean temperature measured with the 4.2 μm sapphire window would be lower, but the result is probably due to trapped air within the asperities which is restricting heat flow at the interface. Results for CB PS were less repeatable.

At t = 0.25 s, the measured temperature for the 4.2 μm surface was lower as expected, but as polymer was cooling further it became higher comparing to surfaces with smaller effective surface area. This behaviour could be explained by the reheat due to polymer part shrinking and detaching from the cavity surface. The effect of the pillars height in case of CB PP showed that temperature was higher for 30 μm pillars at four time steps. In case of CB PS it has repeated the trend of 4.2 μm rough surface, where part was cooling faster initially at t = 0.25 s, following by slower cooling at t = 1 s and t = 1.5 s. The relationship between sapphire surface finish and polymer cooling was not conclusive, moreover the difference in polymer cooling curves was minimal, with maximum standard deviation at four time steps during cooling equal to 1.38 °C for CB PS and 1.68 °C for CB PP.

3.4. Simulated results (conduction solver)

Results from the Moldflow simulation software were compared to the experimentally obtained cooling profiles recorded through the polished sapphire window. As it can be seen in Fig. 10, cooling from simulated results starts from melt set temperatures therefore at t = 0 s temperatures are 220 °C for runs 1 and 5, and 240 °C for runs 9 and 13. Experimentally obtained peak temperatures for CB PP were 140 °C for run 1, 144 °C for run 5, 149 °C for run 9 and 154 °C for run 13. Measured peak temperatures for CB PS were 146 °C for run 1, 152 °C for run 5, 155 °C for run 9 and 159 °C for run 13. From Fig. 10 it can be clearly seen that default value of HTC does not predict polymer cooling well. Large deviations are observed from the start of the cooling until approximately two seconds from the peak recorded value. Increasing the heat transfer coefficient from 2500 W/m^2 C to 7700 W/m^2 C consistently improves cooling profile prediction at different processing conditions. Fig. 10 also shows experimentally obtained and predicted

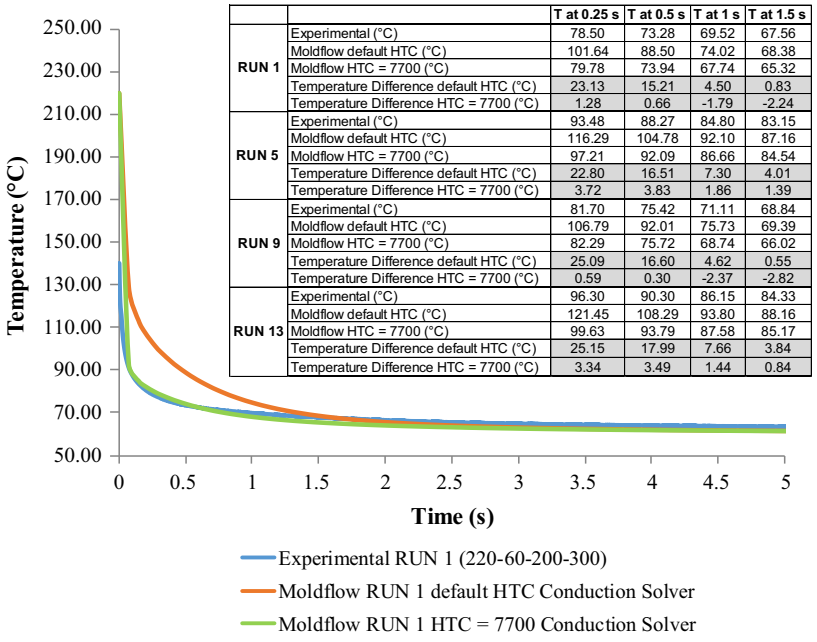

		T at 0.25 s	T at 0.5 s	T at 1 s	T at 1.5 s
RUN 1	Experimental (°C)	78.50	73.28	69.52	67.56
	Moldflow default HTC (°C)	101.64	88.50	74.02	68.38
	Moldflow HTC = 7700 (°C)	79.78	73.94	67.74	65.32
	Temperature Difference default HTC (°C)	23.13	15.21	4.50	0.83
	Temperature Difference HTC = 7700 (°C)	1.28	0.66	-1.79	-2.24
RUN 5	Experimental (°C)	93.48	88.27	84.80	83.15
	Moldflow default HTC (°C)	116.29	104.78	92.10	87.16
	Moldflow HTC = 7700 (°C)	97.21	92.09	86.66	84.54
	Temperature Difference default HTC (°C)	22.80	16.51	7.30	4.01
	Temperature Difference HTC = 7700 (°C)	3.72	3.83	1.86	1.39
RUN 9	Experimental (°C)	81.70	75.42	71.11	68.84
	Moldflow default HTC (°C)	106.79	92.01	75.73	69.39
	Moldflow HTC = 7700 (°C)	82.29	75.72	68.74	66.02
	Temperature Difference default HTC (°C)	25.09	16.60	4.62	0.55
	Temperature Difference HTC = 7700 (°C)	0.59	0.30	-2.37	-2.82
RUN 13	Experimental (°C)	96.30	90.30	86.15	84.33
	Moldflow default HTC (°C)	121.45	108.29	93.80	88.16
	Moldflow HTC = 7700 (°C)	99.63	93.79	87.58	85.17
	Temperature Difference default HTC (°C)	25.15	17.99	7.66	3.84
	Temperature Difference HTC = 7700 (°C)	3.34	3.49	1.44	0.84

Fig. 10. Cooling curves plot of CB PP - experimental and conduction solver results.

temperatures for CB PP at four times steps that were used for statistical analysis of the experimentally obtained cooling profiles. These were t = 0.25 s, t = 0.5 s, t = 1 s and t = 1.5 s starting from peak temperatures. Use of the default HTC value showed that maximum temperature difference was at t = 0.25 s ranging from 22.8 °C to 25.1 °C. An increase of the HTC value showed a reduction of temperature difference in the range of 1.3 °C to 3.7 °C. Similarly to CB PP, there was big temperature difference observed for CB PS at t = 0.25 s when comparing experimental temperature and Moldflow predicted temperature using conduction solver with default HTC values. Prediction of temperature of CB PS at t = 0.25 s, t = 0.5 s, t = 1 s and t = 1.5 s was improved by employing higher HTC value. Improvements in temperature prediction were observed for both materials with conduction solver and HTC equal to 7700 W/m^2 C.

3.5. Simulated results (flow solver)

Results from the Moldflow flow solution were compared to the experimentally obtained cooling profiles recorded through the polished sapphire window. Fig. 11 shows the simulation results when the default HTC values are used. The HTC is in this case assigned three distinct values corresponding to filling, packing and detachment, and some of the features of the temperature curve in Fig. 11 are attributable to the changing HTC value. As described above, the temperature of the polymer surface during the simulation with the flow solver was available through modification of the software, which added an extra result called "Temperature trace". Temperature tracing begins with the start of cavity filling which corresponds to t = 0 s as shown in Fig. 11. However, the central node is located some distance away from the injection location. Fig. 11 demonstrates that polymer melt reaches the central node at t = 0.04 s after the start of the injection. The temperature trace result is meant to be polymer temperature, but the central node is not yet filled with polymer before t = 0.04 s, and so the software outputs a phantom polymer temperature (220 °C) before the node has been filled, which is highlighted with a red circle in Fig. 11.

This phantom temperature should be ignored, and is removed in subsequent analyses.

Fig. 11 shows a reheat of the polymer surface of CB PP at t = 0.068 s and this corresponds with the predicted filling time of 0.067 s, i.e. the end of the filling phase. That the peak pressure is predicted to occur at 0.115 s is suggestive that this is not a compressive heating effect. Moreover, experimental reheating of the surface with an increase of cavity pressure was not observed, as shown in Fig. 12. To investigate this issue, another simulation was performed where the HTC values for filling, packing and

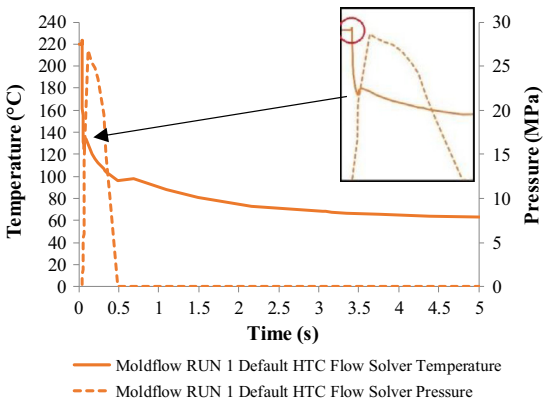

Fig. 11. Moldflow predicted cooling and pressure curves simulated with default HTC values of CB PP.

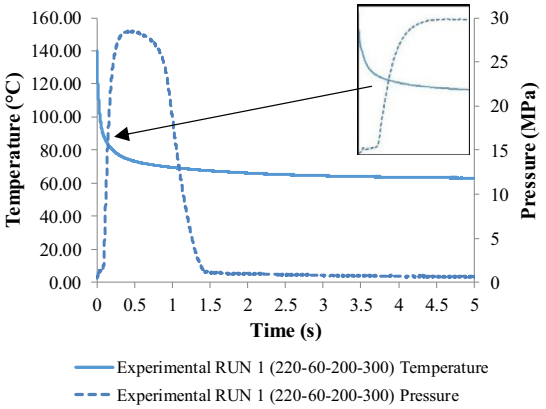

Fig. 12. Experimental cooling and pressure curves of CB PP.

detached phases were set to 5000 W/m^2 C, the default value for the filling phase. This gave a much smaller reheating effect, of 0.32 °C compared with 9.46 °C for the default HTC values.

It is to be expected that a step change in HTC, as arises as the simulation moves between stages, will cause a transient temperature change; this would correspond to a step change in heat flux across the interface and thus a change in *DT/Dt*. A similar effect is seen at the transition between the packing stage and the detached stage. This takes the form of a second reheat, observed at t = 0.487 s and corresponding with the pressure dropping to zero at the same time-step (see Fig. 11). The flow analysis considers that an element has entered into the detached condition when the local pressure has reached zero, whereupon the default HTC value changes from 2500 W/m^2 C (packing) to 1250 W/m^2 C (detached). As the HTC value changes from a higher to a lower value, the solver predicts some reheat at the surface because heat flux at the interface slows down. For simulations with a constant HTC of 5000 W/m^2 C rather than the default conditions, simulation results showed no reheat accompanying the drop of pressure.

Results for CB PS were slightly different. A reheat of 11 °C at the surface was observed at t = 0.0061 s, which corresponded with the end of the filling. However, the second reheat due to the drop of cavity pressure and change to the detached condition was not observed with the default values of HTC. The CB PP drops to zero cavity pressure more quickly at t = 0.487 s comparing to CB PS (t = 1.454 s) and temperatures at those time-steps are different. The core temperature of CB PP when the cavity pressure drops to zero is equal to 173.58 °C, compared with 95.72 °C for CB PS. This justifies why CB PP is subjected to higher reheat when changing from packing phase to detached phase. In the CB PP part there is still a large temperature difference between the core and the skin layer. Heat still flows from the core to the skin, but once HTC is reduced from 5000 W/m^2 C to 1250 W/m^2 C, not as much of the heat leaves the polymer, meaning it accumulates at the skin and generates a reheat of the surface. The reason why the CB PP pressure drops to zero quicker than CB PS lies in the PVT properties of the materials. Density is an important property of materials in the simulation, because it affects both mass and heat transfer. Moreover, density of the polymers varies with pressure and temperature. Thermoplastics have different PVT behaviours across its transition temperature depending on type of polymer. Semi-crystalline polymers have significant and sharp pressure drop due to the sudden decrease in specific volume around transition temperature, whereas amorphous thermoplastics have only a change in slope in its specific volume-temperature curve without a sudden transition from melt to solid [26].

Fig. 13 shows an experimental cooling curve and average of 25 central nodes Moldflow predicted cooling curves. Predicted temperature distributions include the flow solution with default HTC

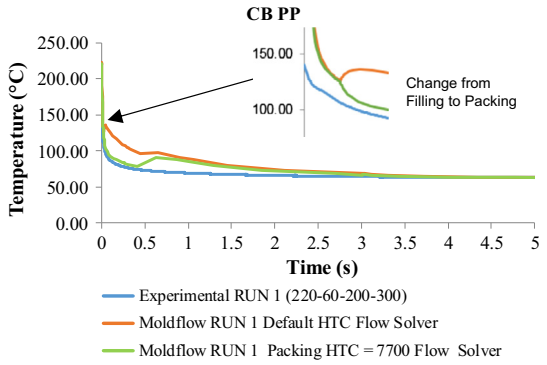

Fig. 13. Cooling curves plot of CB PP - experimental and flow solver results.

values and the flow solution where the packing HTC was changed to 7700 W/m^2 C, keeping filling and detached HTC default. It can clearly be seen that default HTC values do not predict cooling well. On experimental cooling profiles there was no reheat observed, however there was a slight change of slope present which corresponded with end of filling and build-up of the cavity pressure.

Predicted cooling profiles in Fig. 13 demonstrate the effect of HTC values during the change from filling to packing and packing to detached phases. When default values of HTC were used a reheat at the surface can be observed because HTC value for packing phase is lower than filling HTC. On the other hand, an increase of HTC for packing phase changes the slope or one could say increases the cooling rate. A value of 7700 W/m^2 C for the packing phase improves the cooling prediction from the start of the cavity filling till it reaches the detached condition. Maximum reheat during the change from packing to detached phase was 1.7 °C with default HTC values, comparing to 12.19 °C with packing HTC increased to 7700 W/m^2 C. Another simulation with CB PP was performed where filling HTC was kept unchanged, but both packing and detached HTC changed to 7700 W/m^2 C. Results have proved that reheat around t = 0.5 s was purely due to the reduction of HTC value from packing to detached phase. Moreover, no reheating due to the detachment of part was observed experimentally. Elimination of the reheat by setting packing and detached HTC values to 7700 W/m^2 C was also present in run 5, run 9 and run 13.

In case of CB PS a reheat was observed in predicted cooling curves with default HTC values during the phase change from filling to packing. Similarly to CB PP this is an effect of the decrease of HTC value from 5000 W/m^2 C to 2500 W/m^2 C. Experimentally there was no reheat regions observed throughout the cycle. In predicted curves with default HTC values there was no reheat observed during the phase change from packing to detached. As described previously, zero pressure was reached when temperature of the part was close to the mould set temperature. The same trends were observed when different processing parameters were employed in simulation.

Realistically the determined value of 7700 W/m^2 C can be compared only to work of Nguyen-Chung et al. [15] particularly with one of the geometries they have used, namely 12 mm × 11 mm × 0.5 mm rectangular microplate. They have proposed values between 4000 and 6000 W/m^2 C to be used, which agrees with our finding that default value of HTC cannot provide accurate simulation results and higher values have to be used. Comparison with other results can be inadequate since thickness plays an important role in heat transfer. Determined values of HTC in work of Somme et al.,[16] Liu and Gehde [17] and Hong et al. [18] were obtained with geometries of thickness above 1 mm.

4. Conclusions

The cooling of polymers was investigated with respect to simulation of heat transfer at polymer-cavity interfaces during microinjection moulding. Experimental results have shown that polymer cooling during microinjection moulding is very rapid and polymer temperature at the flow front is significantly lower than melt set temperature. By conducting a parametric study and an ANOVA analysis it was possible to identify significant processing parameters on polymer cooling. It was shown that during cavity filling injection speed is a dominant parameter, following by melt and mould temperatures, whereas cavity pressure had a less significant effect. During polymer cooling, mould temperature dominates as the most influential parameter, following my melt temperature. The effects of the processing parameters have followed the same trends for both materials and range of surface topographies. The effects of surface roughness on material cooling were inconclusive as there were no trends observed with an increase of effective surface area. Two cooling solutions within Moldflow simulation software were investigated for prediction of polymer cooling during microinjection moulding cycle. Polymer peak surface temperatures were over predicted when compared to experimentally obtained peak temperatures. Default values of HTC were not able to predict cooling well and showed that the temperature difference between experimentally obtained cooling profiles and predicted values could be as high as 25 °C. A more accurate cooling prediction was obtained with higher value of HTC using the conduction solver. Moreover, the predicted cooling curves for polypropylene and polystyrene were similar, suggesting the results can be generalised to cover both amorphous and semicrystalline thermoplastics with similar properties using the conduction solver. The flow solver has to be used with caution as it requires good understanding of the materials behaviour during the cycle. Some guidance was provided based on experimental results.

The simulation results have shown that the heat transfer coefficient is a significant parameter in the computer simulation of the microinjection moulding. This work suggests that the default values of heat transfer coefficients are unsuitable for microinjection moulding and values in the range 7000–8000 W/m^2 C for both the filling and packing phases will provide more accurate results. Ideally a more sophisticated HTC model could be used in the software to avoid abrupt changes in HTC between each phase in the process, but this could be detrimental to the overall solution time of the simulation.

Acknowledgements

The authors acknowledge the financial support of the EPSRC (EP/I014551/1). Moreover, the first author acknowledges discussions with Dr. F. Costa and Dr. P. Caton-Rose on the simulations with Moldflow software.

Appendix A

Material Temperature Calibration

1. Mould temperature was set to 55 °C and let to thermally stabilise.
2. Mould was closed and polymer injected inside the cavity.
3. Cooling was set to 5 min. During these 5 min mould was closed and polymer thermally stabilised with the mould temperature.
4. Thermal camera was constantly recording digital level units as shown in Fig. 1.

5. After 5 min digital level unit was recorded together with the polymer temperature measured with Kistler p-T sensor which was in contact with the polymer.
6. Temperature of the mould was increased by 5 °C and steps 2 – 5 repeated.
7. Steps 1 – 6 repeated over a temperature range of 55 °C–200 °C at 5 °C increments.

Temperature of the polymer measured with Kistler p-T sensor was used to create calibration curves for the materials as shows in Fig. 14. (See Fig. 15).

Curve fitting algorithm used: 4th order polynomial

4th order polynomial equation for CB PP:

$$CBPPy = -3E - 12x4 + 3E, -08x3 - 0.0001x2 + 0.2064x - 13.89 \quad (7)$$

$R^2 = 0.9995$

4th order polynomial equation for CB PS:

$$CBPSy = -3E - 12x4 + 3E - 08x3 - 1E - 04x2 + 0.1924x - 10.143 \quad (8)$$

$R^2 = 0.9997$

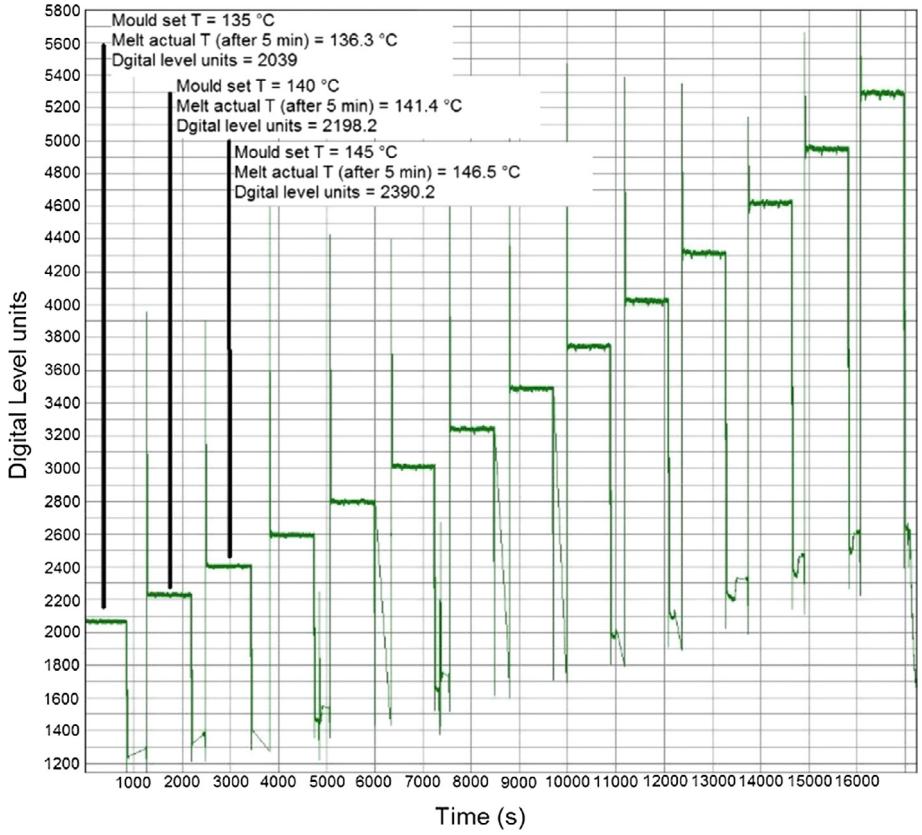

Fig. 14. Polymer temperature calibration result.

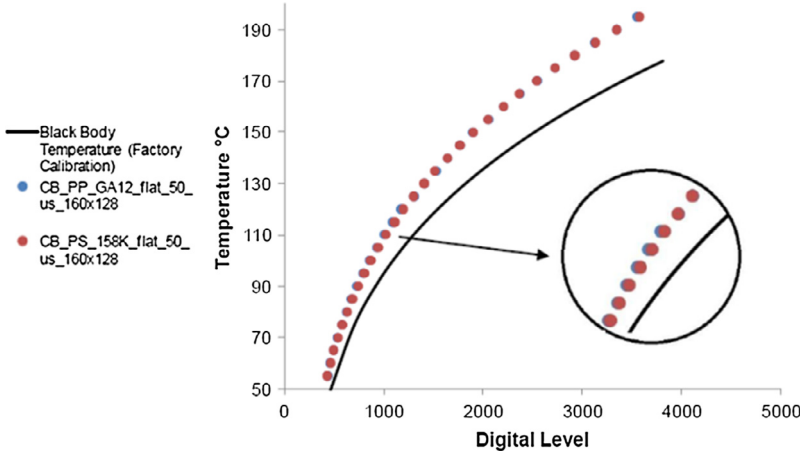

Fig. 15. Temperature calibration curves for CB PP, CB PS and factory calibration for a Black body.

References

[1] B.R. Whiteside, M.T. Martyn, P.D. Coates, G. Greenway, P. Allen, P. Hornsbury, Plast. Rubber. Comps. 32 (6) (2003) 231–239.
[2] C.V. Madhusudana, Thermal Contact Resistance, Springer-Verlag, New York Inc., New York, 1996.
[3] M. Bahrami, J.R. Culham, M.M. Yovanovich, G.E. Schneider, Review of the thermal joint resistance models for nonconforming rough surfaces, Appl. Mech. Rev. 59 (2006) 1.
[4] L. Sridhar, B.M. Sedlak, K.A. Narh, Parametric study of heat transfer in injection molding - effect of thermal contact resistance, J. Manuf. Sci. E. 122 (4) (2000) 698–705.
[5] E.E. Marotta, L.S. Fletcher, Thermal contact conductance of selected polymeric materials, J. Thermophys. Heat. Transf. 10 (2) (1996) 334–342.
[6] K.A. Narh, L. Sridhar, Measurement and modeling of thermal contact resistance at a plastic metal interface, ANTEC'97 (Toronto, Canada), (1997) 2273–2277.
[7] A. Dawson, M. Rides, C.R.G. Allen, J.M. Urquhart, Polymer-mould interface heat transfer coefficient measurements for polymer processing, Polym. Test. 23 (2008) 555–565.
[8] K.A. Narh, L. Sridhar, New Jersey Institute of Technology, Apparatus and Method for Simultaneously Determining Thermal Conductivity and Thermal Contact Resistance, U.S. Pat. 6,142,662 (2000).
[9] Chi J. Yu, J.E. Sunderland, C. Poli, Thermal contact resistance in injection molding, Polym. Eng. Sci. 30 (24) (1990) 1599–1606.
[10] L. Sridhar, K.A. Narh, Computer simulation of the effect of thermal contact resistance on cooling in injection molding, Simulation 73 (3) (1999) 144–148.
[11] D. Delaunay, P. Le Bot, Nature of contact between polymer and mold in injection molding. Part 1: influence of a non-perfect thermal contact, Polym. Eng. Sci. 40 (7) (2000) 1682–1691.
[12] A. Bendada, K. Cole, M. Lamontagne, Y. Simard, A hollow waveguide infrared thermometer for polymer temperature measurement during injection moulding, J. Opt. A-Pure Appl. Op. 5 (2004) 464–470.
[13] A. Bendada, K. Cole, M. Lamontagne, Y. Simard, Analysis of thermal contact resistance between polymer and mold in injection molding, Appl. Therm. Eng. 24 (2004) 2029–2040.
[14] H. Masse, E. Arquis, D. Delaunay, S. Quilliet, P.H. Le Bot, Heat transfer with mechanically driven thermal contact resistance at the polymer-mold interface in injection molding of polymers, Int. J. Heat. Mass Transf. 47 (2004) 2015–2027.
[15] T. Nguyen-Chung, G. Jüttner, C. Löser, T. Pham, M. Gehde, (2010), Determination of the heat transfer coefficient from short-shots studies and precise simulation of microinjection moulding, Polym. Eng. Sci. 2010 165–173.
[16] S.C. Somé, D. Delaunay, J. Faraj, J.-L. Bailleul, N. Boyard, S. Quilliet, Modeling of the thermal contact resistance time evolution at polymer-mold interface during injection molding: effect of polymers' solidification, Appl. Therm. Eng. 84 (2015) 150–157.
[17] Y. Liu, M. Gehde, Evaluation of heat transfer coefficient between polymer and cavity wall for improving cooling and crystallinity results in injection molding simulation, Appl. Therm. Eng. 80 (2015) 238–246.
[18] S. Hong, J. Kang, K. Yoon, Correlation between thermal contact resistance and filling behavior of a polymer melt into multiscale cavities in injection molding, Int. J. Heat. Mass Transf. 87 (2015) 222–236.
[19] F.S. Costa, G. Tosello, B.R. Whiteside, Best practice strategies for validation of micro moulding process simulation, P D Coates and authors, Polymer Process Engineering 09, The University of Bradford, Enhanced Polymer Processing, 2009, pp. 331–364.
[20] B.R. Whiteside, R. Spares, E.C. Brown, K. Norris, P.D. Coates, M. Kobayashi, C.-K. Jen, C.-C. Cheng, Optical imaging metrology for micromoulding cavity flows and products, Plastics, Rubber Compos. Macromole. Eng. 37 (2–4) (2008) 57–66.
[21] S. Bigot, F. Lacan, H. Hirshy, P.V. Petkov, M. Babenko, G.G. Castro, J. Sweeney, H. Ugail, and B. Whiteside, Micro and nano structuring of sapphire for micro injection process investigation, in: 9th International Conference on MicroManufacturing (Nanyang Technological University (NTU) and National University of Singapore, Singapore), 2014.
[22] R. Leach, Fundamental principles of engineering nanometrology, William Andrew, Oxford, 2010, p. 236.
[23] R. Bansal, M. Goyal, Activated carbon adsorption, Taylor & Francis, Boca Raton, 2005, pp. 25–26.
[24] help.autodesk.com, Autodesk Simulation Moldflow insight 2015 Help. [online] Available at: http://help.Autodesk .com/view/MFIA/2015/ENU/ (2015).
[25] 3D flow derivation, Autodesk Moldflow Flex. [online] Available at: https://knowledge.autodesk.com/support/ moldflow-flex/learn-explore/caas/CloudHelp/cloudhelp/2016/ ENU/MoldflowInsight360/files/GUID-C94D0362-421F-4EC1-89A6-931BB8D6D365-htm.html (2015).
[26] H. Zhou, Computer modeling for injection molding, Wiley, Hoboken, N.J., 2013, p. 245.